A System for Remote Measurements of the Wind Stress over the Ocean

W. G. LARGE AND J. A. BUSINGER

National Center for Atmospheric Research, Boulder, Colorado

(Manuscript received 15 June 1987, in final form 10 September 1987)

ABSTRACT

The DISSTRESS system for remote measurements of the surface wind stress over the ocean from ships and buoys is described. It is fully digital, utilizing the inertial dissipation technique. Parallel processing allows anemometer data to be filtered in natural frequency space; that is, the filter cutoffs shift linearly with the mean wind speed of the data to be filtered. The construction of the digital Butterworth bandpass filters is presented in detail.

The performance of the system is evaluated by analyzing the results from 28 days of operation during FASINEX. The mean wind speed is checked, the anemometer response function is established, and drag coefficients are compared to previous studies. The capability of the system is demonstrated by continuous time series of the friction velocity computed every 20 min. The conclusion is that the surface wind stress can be measured more reliably and accurately (20%) with this system than from anemometer wind speeds and a bulk formula.

1. Introduction

The purpose of this paper is to demonstrate the technical feasibility of measuring wind stress over the ocean routinely and reliably from oceanographic ships and buoys. The surface wind stress, τ, is a primary driver of ocean circulation on all scales and is a principal source of drag on the atmosphere. Despite its importance, direct measurements over the ocean are relatively rare and have been used almost exclusively to determine drag coefficients. The parameterization,

$$\tau = \rho C_D U(h) \mathrm{U}(h), \tag{1}$$

where ρ is air density, $U(h)$ the mean wind at a height h in the atmospheric surface layer and C_D the drag coefficient, is the usual method for computing the stress over the ocean on all time and space scales. (See Hellerman and Rosenstein, 1983, and D'Asaro, 1985, for extremes).

The dependence of C_D on h and on the stability parameter, ζ, is given by theory, allowing its equivalent neutral value at $h = 10$ m, $C10_N$, to be used in empirical formulations. When averaged over many determinations, a dependence of $C10_N$ with wind speed emerges (Large and Pond, 1981). Over a few days or more, the random error in bulk stresses from (1) largely disappears and the important errors are systematic due to uncertainty in the $C10_N$ formulation of at least 10% and to the wind speed measurement. On shorter time scales it appears as if (1) often does not hold, as witnessed by calculated drag coefficients from hour averages differing by a factor of 2 from the long-term average (Large and Pond, 1981; Byrne, 1982). Since

$$C10_N = \kappa^2[\ln(z_0/10\ \mathrm{m})]^{-2} \tag{2}$$

where κ is von Karman's constant (0.4), such changes can be attributed to changes in the roughness length, z_0, which in turn appear to be related to the surface wave field.

Therefore, bulk stress estimates are not ideal, and there are two situations in particular where direct stress measurements are preferable. The first is in relating indirect measures such as microwave backscatter (Schroeder et al., 1982) or underwater acoustic noise (Evans et al., 1984) to wind stress, rather than to bulk wind stress through (1). The accuracy of stress estimates from any empirical algorithm is inherently limited by the uncertainty and vagaries of C_D. The second is in studying the short-term ocean response to wind forcing (D'Asaro, 1985) where a factor-of-2 error in the wind stress is important.

It would be most useful to make direct stress measurements from the most common oceanographic platforms, namely ships and buoys, although aircraft can sometimes be used. In the eddy correlation method the stress or momentum flux is obtained from the correlation

$$-\overline{uw} = u^{*2} = \rho^{-1}|\tau| \tag{3}$$

where u and w are the fluctuating downstream and

Corresponding author address: Dr. William G. Large, NCAR/Oceanography Section, Climate and Global Dynamics, P.O. Box 3000, Boulder, CO 80307.

vertical wind components, respectively, the overbar is a time average, and u^* is the friction velocity scaling parameter. This correlation defines the stress, but in practice many different methods of filtering, time averaging, or integrating the cospectrum have been employed to compute it. Such measurements are routinely available from aircraft, but platform motion makes them difficult from buoys and ships. The profile method has been employed from a gyro-stabilized buoy (Dunckel et al., 1974), but not only is this difficult, there appears to be some fundamental problems (Hasse et al., 1977). The inertial dissipation technique is the most attractive for ship and buoy use, because only the mean and frequencies higher than platform motion of the relative horizontal wind past the platform need be measured. This technique has been successfully compared to eddy correlation measurements and employed on oceanographic research ships (Large and Pond, 1981).

2. Methodology

The dissipation method is based on a consideration of the balance of turbulent kinetic energy, which in steady, homogeneous flow becomes (Busch, 1977) $\epsilon = P + B - D_V$, where ϵ is molecular dissipation, P the mechanical production, B buoyant production, and D_V is a divergence term that can be neglected in this application as discussed by Large (1979). The inertial form of the method infers ϵ from measurements of the spectral density of the downstream velocity, $\Phi_u(f)$, at frequencies f in the inertial subrange, where the Kolmogoroff hypothesis predicts

$$\Phi_u(k) = \Phi_u(f)df/dk = K'\epsilon^{2/3}k^{-5/3} \tag{4}$$

with $K' = 0.55$, the one-dimensional Kolmogoroff constant. Assuming Taylor's hypothesis gives the wavenumber $k = 2\pi f/\mathrm{U}$, where U is the mean relative wind speed past the measurement point.

By definition, at the height of the Monin–Obukhov length, L, the mechanical production in the equivalent neutral case, P_0, equals B, and an appropriate stability parameter is

$$\zeta = h/L = -B/P_0.$$

A method of estimating ζ from the mean wind speed, air temperature, sea temperature, and measurement height is given and tested in Large and Pond (1982). Dimensional analysis suggests

$$\frac{\kappa h}{u^*}\partial_h U = P/P_0 = \phi_m(\zeta) \tag{5}$$

for heights above the direct influence of boundary protuberances such as ocean surface waves and below about 2.8 s times the mean wind speed. This upper bound is the extent of the constant flux layer, where the stress has decreased by 10% from its surface value (Lumley and Panofsky, 1964). The right-hand side of (5) has been empirically determined and Panofsky and Dutton (1984) discuss several acceptable formulations, including

$$\phi_m(\zeta) = \begin{cases} 1 + A_1\zeta & 0 < \zeta < 0.2 \\ (1 - A_2\zeta)^{-1/4} & -1.0 < \zeta < 0. \end{cases}$$

They give $A_1 = 5$ and $A_2 = 16$, but setting $A_1 = 7$, as suggested by Yaglom (1977), gives the best fit to over ocean data (Large and Pond, 1982). By comparison with simultaneous eddy correlation measurements, Large and Pond (1981) found the best inertial dissipation estimates of u^* over the ocean to be given by

$$u^{*3} = \kappa h\epsilon F_2(\zeta), \tag{6}$$

with a stability correction function of

$$F_2(\zeta) = [\phi_m(\zeta) - \zeta]^{-1}. \tag{7}$$

The turbulent kinetic energy budget is not understood well enough for use in evaluating the accuracy of these estimates (Fairall and Larsen, 1986). However, this comparison indicates that it is possible to achieve an accuracy of 10% in u^*, or 20% in stress.

The stability correction ranges from about 0.85 to 1.14 over the stability range where (6) has been tested, $-0.6 < \zeta < 0.05$. Thus, the correction to u^* is at most 5% and it is usually adequate to have a remote system compute neutral u^* values [$F_2(0) = 1.0$] and apply a bulk stability correction later if necessary.

The difficult measurement is that of the spectral density within the inertial subrange. This subrange is fixed in natural frequency space

$$n = \frac{kh}{2\pi} = \frac{fh}{U}. \tag{8}$$

Therefore, it is advantageous and natural to calculate spectral density over fixed bandwidths in n-space, from n_1 to n_2, and hence in wavenumber-space for fixed h, by allowing the frequencies to float according to (8). Thus, the frequencies being measured increase linearly with wind speed. From the integral of the left-hand side of (4) in n-space,

$$G(n_1, n_2) = \int_{n_1}^{n_2} \Phi_u(n)dn, \tag{9}$$

it is straightforward to calculate the dissipation rate from

$$\epsilon^{2/3} = \frac{2}{3K'}\left(\frac{2\pi}{h}\right)^{2/3}(n_1^{-2/3} - n_2^{-2/3})^{-1}G(n_1, n_2), \tag{10}$$

and hence u^* from (6) and the stress from (3).

The inertial subrange begins at about $n = 0.2$, so setting $n_1 > 0.25$ insures that the spectral integrals always contain energy only from the subrange. The upper limit of the subrange is beyond the response of most sensors, so it is not a design factor.

In practice, several values, $G_j(n_1, n_2), j = 1, N_F$ should be found, at least when first testing new instrumenta-

tion, because they allow for the $k^{-5/3}$ or $f^{-5/3}$ behavior of the inertial subrange (4) to be checked. Typically, radio interference or physical obstructions upwind tend to increase the high frequencies more than the lower. On ocean platforms, wave motion can contaminate the lower frequencies of the subrange. In situations where the measurements are known to be reliable the multiple spectral values allow for the frequency response of the sensor to be determined under actual measurement conditions, as in Pond et al. (1979).

3. The DISSTRESS system

The basic components of the DISSTRESS system for measuring the surface wind stress with the inertial dissipation technique are shown in Fig. 1. A Gill propeller-vane anemometer (GPVA) is used because of its proven performance. It is extremely robust, operates in all weather conditions, requires minimal maintenance, and has excellent calibration linearity and stability. With the 27106X optical encoder model, the anemometer output is a pulse train, whose frequency is directly proportional to the wind speed:

$$f_a = UCN_w, \tag{11}$$

where N_w is the number of windows in the optical chopping disk and C the propeller calibration in revolutions per second per millimeter per second of wind. The calibration, C, depends only on the pitch of the helicoid propeller and even rather severe ablation of the blades does not change it. The pitch-derived calibrations provided by the manufacturer are accurate to within 2%. Although careful wind tunnel calibration could improve the accuracy to about 0.5%, this extra effort is not necessarily required in order to achieve 10% accuracy in u^*.

A disadvantage of the GPVA is that corrections to inertial dissipation estimates of u^* are required in order to account for a lack of sensor response, even using the fast response polystyrene propellers. Therefore, the sensor response function must be well known. To first order it can be modeled as a single pole, low-pass filter (R-C circuit) with a transfer function

$$|H|^2 = \frac{\Phi'_u(f)}{\Phi_u(f)} = \left[1 + \left(\frac{2\pi D}{U} f\right)^2\right]^{-1} \tag{12}$$

where f is frequency, D the distance constant and $\Phi' u(f)$ the reduced spectral density output from the anemometer. However, D appears to vary with propeller type and wind speed, so it is necessary to establish its behavior with each new system. From (12) the sensor response correction to u^* is

$$F^* = [1 + (2\pi Df/U)^2]^{1/2},$$

$$\partial F^*/F^* = (2\pi Df/U)^2 F^{*-2} \partial D/D, \tag{13}$$

where $\partial F^*/F^*$ and $\partial D/D$ are the fractional errors in F^* and D, respectively. In order to achieve a 10% accuracy in u^*, it is necessary to keep the error in F^* to less than 5%. Previous work (Large, 1979) indicates that the distance constant of a GPVA can be determined to within 25%, which sets the following requirement:

$$Df/U = Dn/h < 0.1. \tag{14}$$

Thus, $n_2(N_F)$, the highest upper limit of integration (9), should be set to satisfy (14).

The primary purpose of the wind processor is to decode the anemometer pulses into wind speed samples, u_m, and to load, alternately, wind data stacks A and B with sets of N wind samples, $\{u_m, m = 1, N\}$, and the mean over the samples, U. The number of samples is set by the basic sampling interval, T_s, and the sampling rate R, such that $N = RT_s$. The wind processor also monitors the relative wind direction from the GPVA's vane direction potentiometer and sends a 16-bit direction word to the wind data stack. The nature of this word can change with application; some examples are a combined 8-bit minimum plus an 8-bit maximum relative wind direction, or mean wind direction, or wind steadiness.

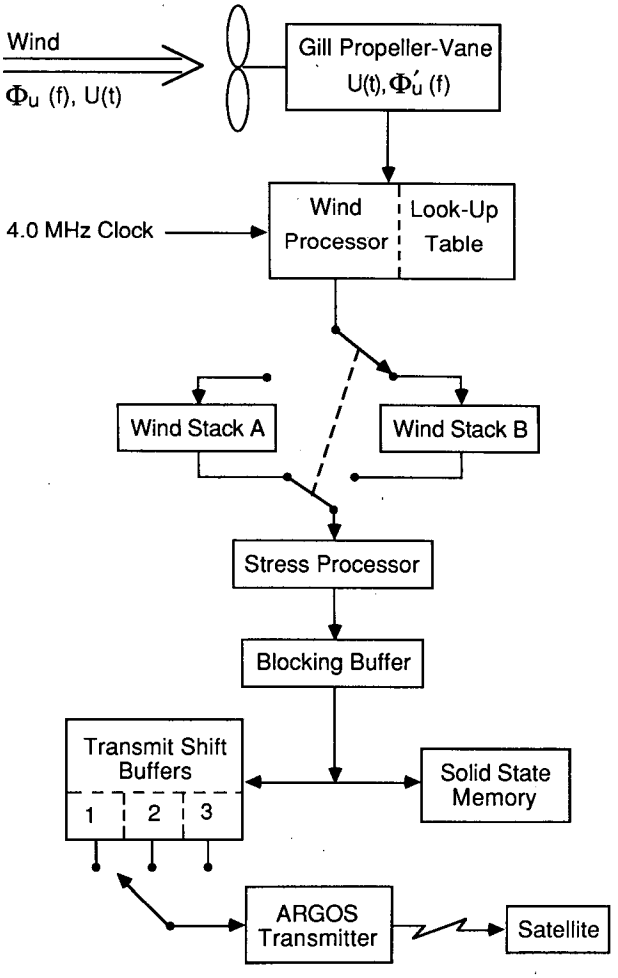

FIG. 1. Basic components of the DISSTRESS systems for measuring the wind stress magnitude with the inertial dissipation technique.

The pulse decoding proceeds as follows: When a sample is requested the processor waits for the next rising edge of the pulse train, then counts the number of peaks on a high frequency clock that occur before the next rising edge. The number of counts, N_c, is then used to reference storage location N_c of a look-up table in the processor, which contains a 16-bit integer number corresponding to the wind speed in millimeters per second. This integer is sent to a data stack as u_m and also is accumulated for the mean wind speed calculation. Storage location N_c of the table contains the integer

$$u = f_c(N_c C 1.005 N_w)^{-1}, \tag{15}$$

where f_c is the clock frequency and the factor 1.005 converts the total horizontal wind speed as measured by the anemometer to the downstream component (Pond et al., 1979). In the case of 19 cm, four-bladed propellers with 30 cm pitch, $C = 3.402 \times 10^{-3}$, $N_w = 15$, and $f_c = 4.0$ MHz,

$$u \approx 78 \times 10^6 N_c^{-1}.$$

For operation at mean wind speeds from 2.5 to 50 m s^{-1} the minimum and maximum wind speeds should be about $3\sigma_u$ below 2.5 m s^{-1} and $3\sigma_u$ above 50 m s^{-1}, or 1.75 m s^{-1} and 65 m s^{-1}, respectively, since $\sigma_u \approx 0.1U$. This range is covered by the look-up table, which is loaded according to (15) with 65 535 (65.535 m s^{-1}) in its lowest storage location (1190), and with 1587 (1.587 m s^{-1}) at its top (49 151).

The timing of the data processing is displayed in Fig. 2. During odd intervals, wind data stack A is filled by the wind processor, while the stress processor is operating on wind stack B, and vice versa during even intervals. Over each interval the stress processor calculates $j = 1, N_F$ values of the dissipation, $\{(\epsilon_j)_i, i = 1, N_I\}$. It accumulates each value and the mean wind from the processor over a period T_p, corresponding to N_I intervals, whereupon averaging of these values is performed. The N_F average dissipation values are converted into N_F neutral u^* values (6), which are combined with the mean wind and the wind direction word to form a dataset $\{S_p, p = 1, N_P\}$ of $N_F + 2$ 16-bit words. This dataset is sent to a blocking buffer and after every N_P periods an additional 16-bit time word is added to the buffer to form a block of $N_P(2 + N_F) + 1$, 16-bit words. A block is then copied both to solid state memory and to the lowest of three transmit buffers. Old data are shifted to the next highest buffer until they are finally lost from buffer 3. The transmit-shift buffers only keep the last 256 bits of each block, because this is the maximum allowable length of an ARGOS data transmission. A data block is transmitted every 2 min, but it is received only when there is an ARGOS receiving satellite overhead. Under these constraints, more data blocks are received at least once, if each is transmitted over a longer period of time by reducing the frequency. Therefore, the transmitter is loaded from a different transmit buffer at the beginning of every odd interval, according to the sequencing shown in Fig. 2. In this way, each block of data is transmitted periodically over

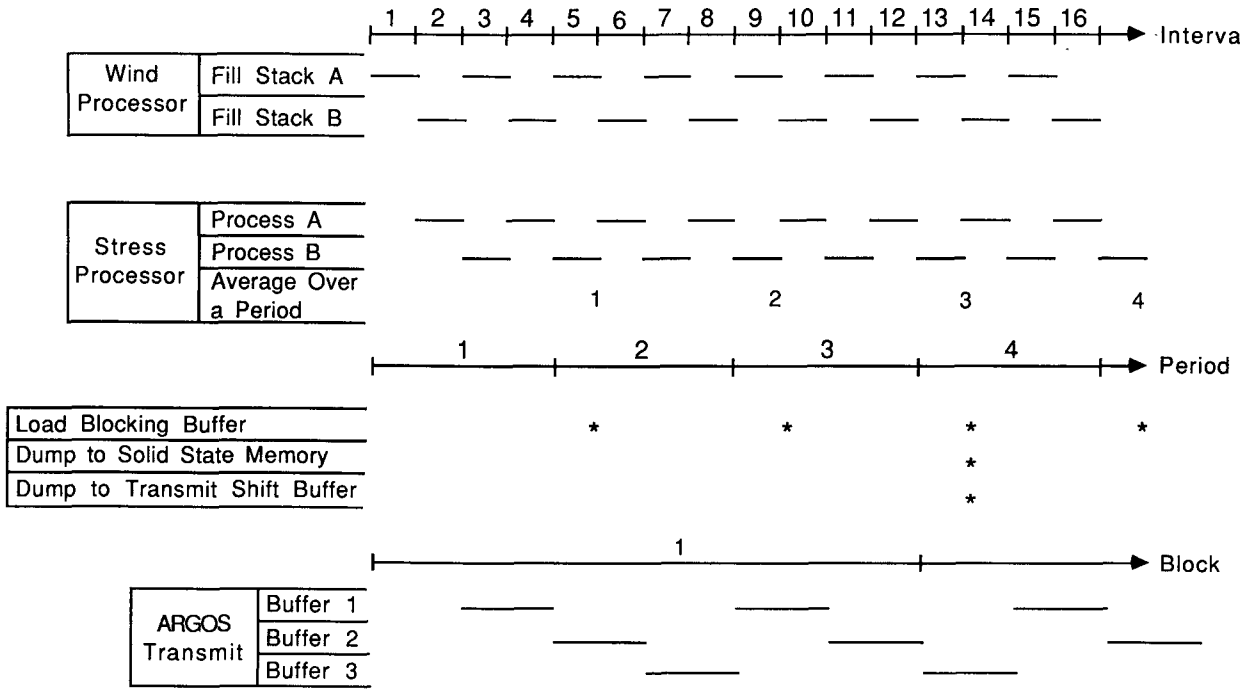

FIG. 2. Timing of the processing, data storage, and data transmission in the DISSTRESS system.

a three-block period of time, first from buffer 1, then from buffer 2, and finally from buffer 3. Since an ARGOS receiver can accommodate many tens of transmitting platforms in its field of view at any one time, a DISSTRESS system could be operated as one component of a larger system.

4. Stress processing

The majority of software and computations in the stress processor are concerned with determining the N_F integrals of reduced spectral density from a stack, A or B, of N wind speed samples. These values are obtained through repeated digital bandpass filtering (N_F times) of the input wind sequence $\{u_m\}$, passing frequencies from $n_1(j)$ to $n_2(j)$ and using the filter outputs $\{y_m, m = 1, N\}$ to approximate the integral (9) through Parseval's relation,

$$N^{-1} \sum_{m=1}^{N} y_m^2 = G_j(n_1, n_2). \quad (16)$$

All bandpass filters consist of a high-pass stage of order M_H, and cutoff frequency $f_1(j)$, and of a low-pass stage of order M_L and cutoff frequency $f_2(j)$, with $f_1(j) < f_2(j)$. Butterworth filters are employed for both stages, because they are maximally flat in the passband.

For each processing interval, the mean wind and the internally stored measurement height h define the frequency space cutoffs

$$f_1(j) = Un_1(j)/h; \quad f_2(j) = Un_2(j)/h.$$

The bandpass construction for each filter j then proceeds as follows: First, f_1 is used to create a high-pass filter sequence of $s = 1, M_H/2$ second-order filter sections. Second, f_2 is used to create a low-pass filter sequence of $s = 1, M_L/2$ second-order filter sections. (When the order for either stage is odd, the second-order sequence is $s = 1, (M - 1)/2$, and one first-order section is added.) Third, the two sequences are combined into one filter sequence of $s = 1, M$ [$M = (M_H + M_L)/2$] second-order sections. For each of these sections the second-order recursive digital filter,

$$u_m(s) = c_0 u_m(s-1) + c_1 u_{m-1}(s-1) + c_2 u_{m-2}(s-1) + d_1 u_{m-1}(s) + d_2 u_{m-2}(s), \quad (17)$$

is applied to the output from the previous filter section, denoted as $u_m(s-1)$, such that $u_m(0)$ is the original input and $y_m = u_m(M)$ is the ultimate output. The coefficients of (17) are functions of the cutoff frequency $f_c = f_1$ or f_2, the section s, the filter order, $M_S = M_H$ or M_L, and the sampling rate R. Therefore, they must be recomputed for each of the M sections of all N_F filters, using the measured U from each processing interval.

The following describes both the implementation of (17), including a straightforward, efficient means of determining the required filter coefficients, and how the recursive digital Butterworth filtering is performed within the stress processor. The basic algorithm computes the coefficients of a second-order section, s, of either the high- or low-pass stages. The procedure follows Hamming (1983) and the basic steps are as follows:

1) The tangent half-angle substitution and the Nyquist frequency, $R/2$, are used to rescale the frequencies $[0, R/2]$ to $[0, \infty]$. The cutoff frequency is thereby transformed to a rescaled frequency

$$w_c = \tan(\pi f_c/R).$$

2) The fundamental representation of either a Butterworth low-pass filter

$$H_L(w) = [1 + (w/w_c)^{2M_L}]^{-1}$$

or a Butterworth high-pass filter

$$H_H(w) = 1 - [1 + (w/w_c)^{2M_H}]^{-1}$$

is implicitly created, with the bilinear transformation

$$w = (-1)^{1/2}(1 - z)(1 + z)^{-1},$$

replacing w with an expression in complex z.

3) The resulting expression is expanded (implicitly) into a product of $M_S/2$ terms of the form

$$(a_3 z^2 + a_2 z + a_1) \quad (b_3 z^2 + b_2 z + b_1)^{-1}, \quad (18)$$

each of which corresponds to one sequence, s, of the second-order filter sections.

4) The coefficients of (18) are assigned:

$$a_1 = a_3 = 1.0(\text{high} - \text{pass}) \text{ or } w_c^2(\text{low} - \text{pass})$$

$$a_2 = -2.0(\text{high} - \text{pass}) \text{ or } 2w_c^2(\text{low} - \text{pass})$$

$$b_1 = w_c^2 + 1 - 2w_c \sin[\pi(2s-1)/2M_S]$$

$$b_2 = 2.0(w_c^2 - 1)$$

$$b_3 = w_c^2 + 1 + 2w_c \sin[\pi(2s-1)/2M_S].$$

5) The second-order recursive filter (17) has the transform function

$$H(f) = (c_0 z^2 + c_1 z + c_2)(z^2 - d_1 z - d_2)^{-1} \quad (19)$$

and the coefficients are, from inspection of (18),

$$c_0 = a_3/b_3, \quad c_1 = a_2/b_3, \quad c_2 = a_1/b_3,$$
$$d_1 = -b_2/b_3, \quad d_2 = -b_1/b_3.$$

In general, such filtering can also be represented by the matrix multiplications

$$X_{m+1}(s) = AX_m(s) + Bu_m(s-1), \quad \text{memory update}$$

$$u_m(s) = CX_m(s) + Du_m(s-1), \quad \text{section output}$$

where

$$A = \begin{pmatrix} 0 & 1 \\ d_2 & d_1 \end{pmatrix}$$

$$B = \begin{pmatrix} 0 \\ 1 \end{pmatrix}$$

$$C = (c_2 + c_0 d_2, c_1 + c_0 d_1) \quad D = c_0$$

produce the equivalent of (17). Since only five of the matrix elements are neither 0 nor 1, only five multiplications are required for each element of the input sequence. Figure 3 is a pictoral representation of the workings of a section, showing the feedbacks and the role of each coefficient.

Since the span, or number of simple multiplications per data point, of a second-order section is 5, there are $(5MN)$ multiplications per filter. Therefore, the total number of multiplications per processing interval required to compute (16) is

$$\text{BPF} = N_F(5MN + N). \tag{20}$$

An alternative method of computing spectral density at discrete frequencies up to the Nyquist frequency is the fast Fourier transform (FFT). At best, for N a power of 2, the Fourier coefficients can be computed with $N \log_2 N$ complex multiplications or $4N \log_2 N$ simple multiplications. Since these coefficients need to be squared, the number of multiplications required to compute an integral over spectral density is about

$$\text{FFT} = 4N \log_2 N + N. \tag{21}$$

Table 1 shows the ratio of bandpass filter operations to FFT operations, BPF:FFT, for a range of possible operating parameters.

5. FASINEX

The DISSTRESS system was first operated during the Frontal Air–Sea Interaction Experiment (FASINEX), on board the R/V *Endeavor* from 11 February to 10 March 1986. Although its performance was continually monitored, no maintenance was required over the 28 days. A GPVA with 19 cm, 4-blade propellers was installed 13.5 m above the sea surface and 11 m above the deck of the ship. The mast rose directly above the bow about 15 m foreward of the smoke stacks and 20 m forward of the bridge. Since the mast itself offered no obstruction to the wind, severe flow interference due to the wake effects was expected only from the ship, at relative wind directions greater than 120 deg from head on. Otherwise, the measurements were made at least two body diameters upstream from any flow disturbing elements, so the measured $\Phi_u(f)$ should be well within 10% of its far upstream value (Wyngaard, 1981). The ship carried out a wide variety of meteorological and oceanographic programs in the area bounded by 27° and 29°N, 67° and 71°W (Fig. 4). Every effort was made to accommodate the stress measurements, but the other activities often necessitated ship headings, maneuvers and radio communications that interfered with the DISSTRESS measurements.

The system's operating parameters during FASINEX are given in Table 2. Aliasing of higher frequencies into the highest passband was avoided by setting the sampling rate, R, to twice the highest frequency to be passed:

$$R = 2[50n_2(N_F)/h] = 10 \text{ Hz},$$

with 50 the design maximum wind speed in meters

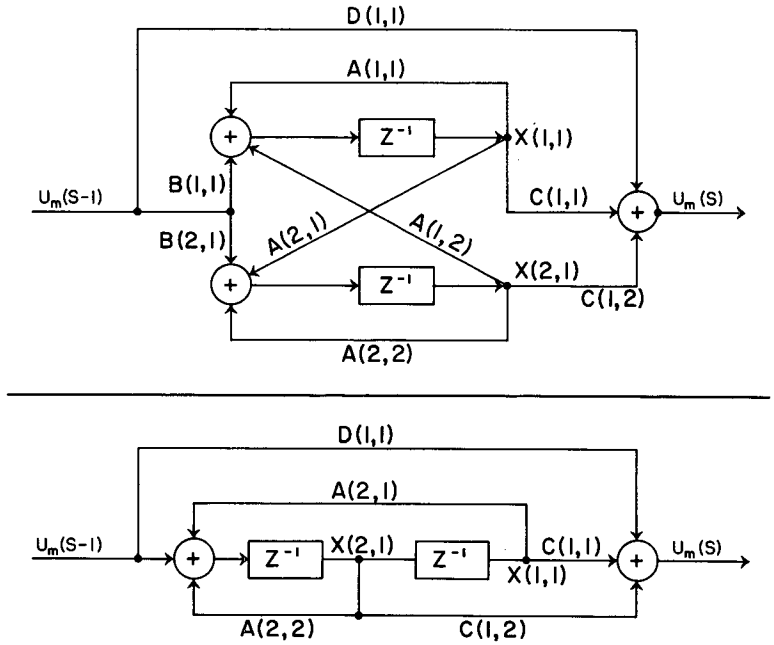

FIG. 3. Pictoral representations of the working of a second-order Butterworth filter section, showing feedbacks and the role of each coefficient. The general matrix multiplications are shown in the upper panel, while the specific matrix multiplications in the stress processor are shown in the lower panel.

TABLE 1. Ratio of the number of simple multiplications required using a digital bandpass filter to those required by a fast Fourier transform technique for a range of possible operating parameters.

			BPF:FFT		
N	$\log_2 N$	N_F	$M = 4$	$M = 6$	$M = 8$
1024	10	1	0.5	0.8	1.0
		3	1.5	2.3	3.0
4096	12	1	0.4	0.6	0.8
		3	1.3	1.9	2.5
16 384	14	1	0.4	0.5	0.7
		3	1.1	1.6	2.2

per second, and $n_2(N_F)/h = 0.10$ according to (14). A period was chosen to be the time required to smooth the influence of atmospheric boundary layer plumes and downdrafts and produce statistically steady u^* estimates, namely, 20 min (Khalsa, 1980). The number of wind samples in an averaging interval, $N = 3000$, is a compromise between the desire to reduce noise, and the number that can be conveniently stored in the wind data stacks and processed. The basic averaging interval is then 300 s = 5 min, giving $N_I = 4$ intervals per period.

For this first deployment N_F was set to 3, so the sensor response could be established. The validity of the approximation (16) was checked prior to FASINEX by comparison with FFT results using simulated data. For filter order ≤ 3, (16) was consistently larger. A good comparison was found for filter orders between 6 and 10, and $M_H = M_L = 6 = M$, was chosen to minimize the computations. Even so, with these parameters Table 1 shows that the bandpass filtering requires about twice as many multiplications as would an FFT procedure. However, it is likely that because the wind spectrum falls off as $f^{-5/3}$, and because of sensor response falloff, an optimal scheme would have $M_L < M_H$, with perhaps $M_H = 6$, $M_L = 2$, and $M = 4$. Then once the sensor response was established, $N_F = 1$ or $N_F = 2$ would be adequate, making the number of bandpass multiplications only 0.4 or 0.8 times those of an FFT, respectively (Table 1).

In order for all the data to be transmitted via ARGOS, N_P was set to 3, giving 256 bits per 1-h block. The anemometer height of $h = 13.5$ m sets $n_2(3) = 1.3$ to satisfy (14). Filter j is useful only at wind speeds greater than $U_{\min}(j) = f_s(U_{\min})h/n_1(j)$, where $f_s(U_{\min})$ is the high frequency limit of the platform motion. At $U = 20$ m s^{-1}, f_s is about 0.3 Hz (Large, 1979). Even with no wind there may be some swell with $f_s = 0.17$ Hz. A linear fit to these two extremes gives

$$U_{\min}(j) = 0.17 \text{ Hz} \quad [n_1(j)/h - 0.0065 \text{ m}^{-1}]. \quad (22)$$

In order to have at least one filter operate down to $U = 2.5$ m s^{-1}, $n_1(3)$ was set to 0.97, as was $n_2(2)$, which keeps filter 2 independent of filter 3. For filter 1 to operate down to $U = 10$ m s^{-1}, $n_1(1)$ was set to 0.32. The midpoint between $n_1(1)$ and $n_2(2)$ gives $n_2(1) = n_1(2) = 0.65$, and satisfies filter independence.

The first test of system performance was a comparison of the 20 min average wind relative to the GPVA to that from a Gill propeller bi-vane (GPBV) operated by the Naval Postgraduate School (NPS). The GPBV was mounted about 2 m ahead of the *Endeavor*'s bowmast at a height of 10 m. Figure 5 shows that the GPVA speeds tend to be greater than those from the GPBV by just about the amount expected due to the height difference. The remaining bias is well within the 2% calibration accuracy. The scatter is not large and can be attributed mostly to nonsimultaneous averaging times, although some statistical turbulent fluctuation

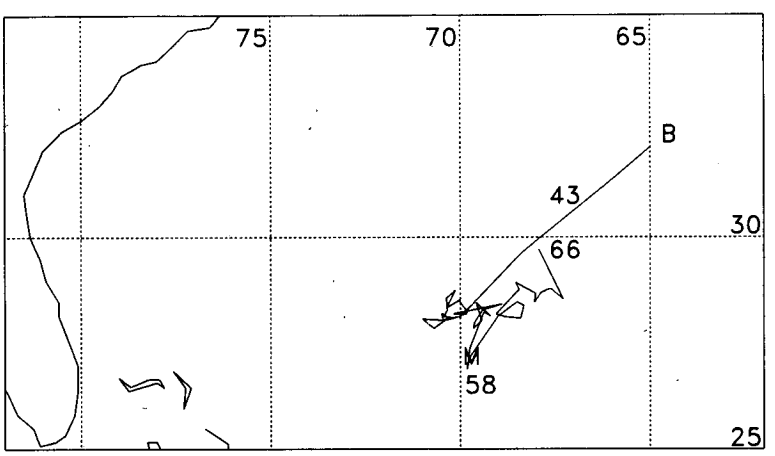

FIG. 4. Shiptrack joining positions of R/V *Endeavor* every 12 h during FASINEX from its Bermuda (B) departure until heading back to Woods Hole, MA. Positions at 1200 UTC; 1986 year days 43, 58, and 66 are shown as in the location of the FASINEX moored array (M). The grid annotations are in degrees north latitude and degrees west longitude.

TABLE 2. DISSTRESS system operating parameters during FASINEX.

R	10 Hz, sampling rate
T_P	20 min, periods
N	3000, wind samples
T_S	300 s = 5 min, sampling interval
N_I	4, intervals per period
N_F	3, bandpass filters
$M_H = M_L$	6, high- and low-pass filter orders
N_P	3, periods per block
T_b	1 h, blocks
h	13.5 m, anemometer height

Filter j	$n_1(j)$	$n_2(j)$	$F^*(j)$	$U_{\min}(j)$
1	0.32	0.65	1.03	10 m s^{-1}
2	0.65	0.97	1.08	4 m s^{-1}
3	0.97	1.30	1.16	2.5 m s^{-1}

is expected. From Fig. 5 it appears as if the GPVA performed properly, at least in determining the mean wind.

An evaluation of the GPVA response again indicated that the distance constant is a function of wind speed:

$$D = 0.4mU \quad (U - 2.0 \text{ m s}^{-1})^{-1}. \qquad (23)$$

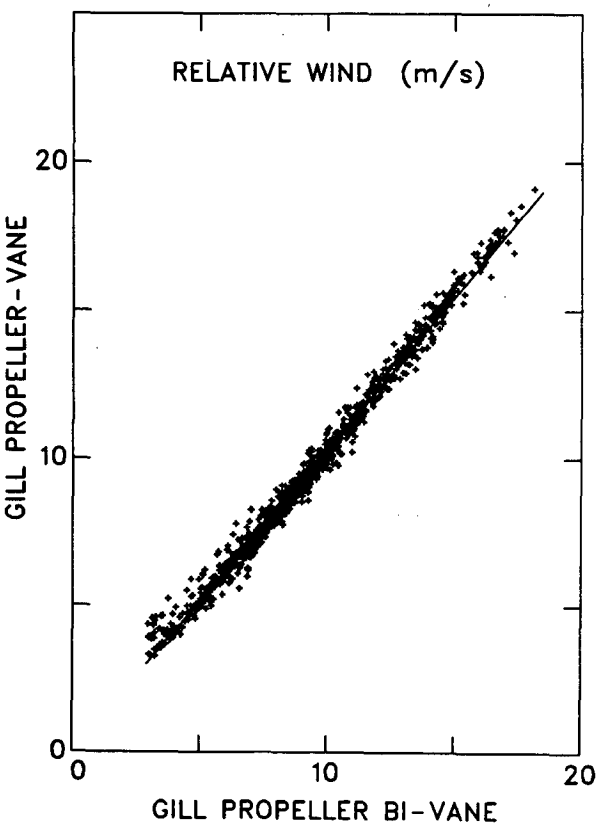

FIG. 5. Comparison of hourly averaged wind speed relative to the Gill propeller-vane and the Gill propeller bi-vane anemometers. The solid line of slope 1.03 represents the relationship expected because of the anemometer height difference in neutral stratification.

Compared to previous results where a similar propeller drove a dc generator, this response is somewhat poorer at low winds, but much better at high winds. Figure 6a shows u^* values from filters 2 and 3 before sensor response corrections have been applied. As expected, the values from the higher frequency filter tend to be lower. After correcting according to (12), the bias is no longer evident, at least for $u^* < 0.5$ m s^{-1} (Fig. 6b). In general, the corrected u^* from both filters agree to well within the 10% indicated by the dashed lines in Fig. 6b. Thus, there is no reason to suspect that the goal of 10% accuracy in u^* cannot be met.

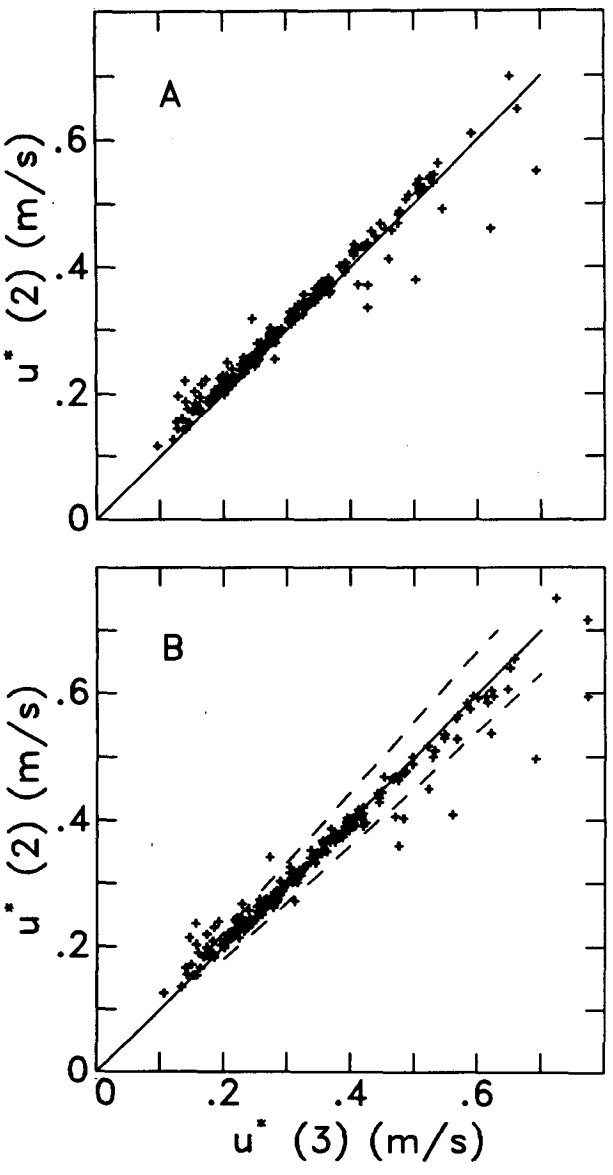

FIG. 6. Comparison of friction velocity computed from two different frequency bands in the inertial subrange, both (A) before and (B) after correcting for sensor response. The dashed lines in (B) indicate a 10% difference.

There are some cases where $u^*(3)$ is much larger than $u^*(2)$ and vice versa. The former may indicate flow or radio interference. The latter suggest some ship or mast motion. In both cases the data from such a period are rejected automatically on the basis of no inertial subrange. The criterion used is that spectral values should all fall within 10% of an average $f^{-5/3}$ slope, which corresponds to each $u^*(j)$ value differing by less than 5% from their overall average.

A single u^* value from reliable filters is computed as the cube root of the average of $u^*(j)^3$, so that the averaging is effectively of the dissipation rates, ϵ_j. The resulting u^* should be adequate for many purposes and produce more accurate stresses than (1). Of course once (23) is established for a particular system, the response corrections could be applied in the stress processor, as could be the filter selection subrange check and dissipation rate averaging in systems with $N_F > 1$. Thus, quality controlled neutral u^* values could be both stored and transmitted in real time via ARGOS for operational use.

In order to improve the accuracy and avoid a systematic error, the stability correction should be made to u^* whenever possible. In FASINEX the sea and air temperatures and the relative humidity were recorded routinely by the NPS system. For stability and also drag coefficient computations, the true mean wind speed, U_t, is also required. However, it cannot always be calculated very well, because of flow interference and the difficulty in obtaining a good measure of the ship's velocity, $\mathbf{V}_s$. It is found from

$$U_t = |\mathbf{U}_t|,$$

where

$$\mathbf{U}_t = \mathbf{U} + \mathbf{V}_s,$$

and $\mathbf{U}$ is the vector wind relative to the GPVA. Since u^* estimates depend only on $U = |\mathbf{U}|$, they are, in many ways, easier to obtain than the true wind speed.

The *Endeavor*'s SAIL system periodically logged the ship's speed and heading, but these were found to be inadequate for calculating $\mathbf{V}_s$. Instead, ship positions from both satellite navigation and LORAN at the beginning and end of each period were differenced to give an average $\mathbf{V}_s$. Navigational drift and errors made this a complicated procedure and when all things are considered, U_t has an uncertainty of at least 10% and occasional errors of a few meters per second or more. This situation is true of any ship wind and illustrates a serious problem in calculating stress from ship winds using (1), namely the removal of the ship's velocity from its anemometer signal.

The ensemble average of many drag coefficients tends to converge to a smooth, relatively well established function of wind speed (Fig. 7, solid line). Therefore, coefficients calculated from the DISSTRESS system's u^* values and from U_t (10 m) and ζ can be used to evaluate the system's performance. The overall scatter in Fig. 7 of $C10_N$ from FASINEX vs the 10 m

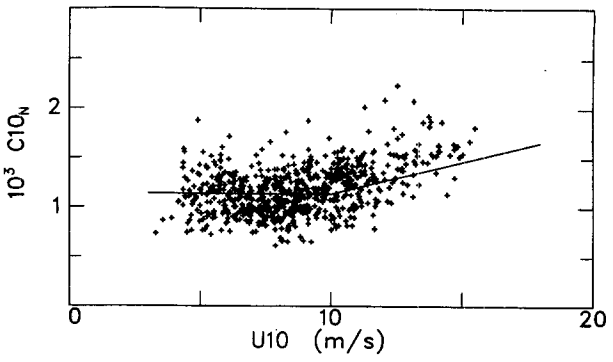

FIG. 7. Neutral 10-m drag coefficients as a function of wind speed from the DISSTRESS system during FASINEX. The solid line is the formulation in Large and Pond (1981).

wind speed is reminiscent of other datasets, which are compared in Table 3, for $U10_N < 10$ m s^{-1}, where there is no significant trend with wind speed. The DISSTRESS results from FASINEX are remarkably consistent, indicating that this automated system is able to measure both the mean and fluctuations of the wind stress as well as previous instrumentation.

As an example of the data product the DISSTRESS system is capable of producing, time series from year days 43 and 44 (12 and 13 February) 1986 are shown in Fig. 8. On these days R/V *Endeavor* was steaming into the wind at 8 to 10 kt on its way to the FASINEX site. With minimal ship maneuvers and a favorable relative wind direction, the u^* data return is 93%, and there is at least one period in each hour with a good u^*. On year day 45, FASINEX oceanographic work began in earnest and more than 50% of the periods were contaminated. As stated earlier it is more difficult to obtain $U10$ and even on day 44 it is available from only 64% of the periods. A remarkable feature of the u^* time series is the very small (less than 10%) period-to-period fluctuations. It demonstrates that a 20-min average is sufficient to produce statistically steady u^* estimates. Again from Fig. 8 there is no evidence to suggest that the goal of 10% accuracy in u^* cannot be achieved.

The drag coefficient is proportional to the square of the u^*:$U10$ ratio, and even so $C10_N$ is a relatively smooth function of time over several hours. Although much of the period-to-period variability can be attributed to u^* and $U10$ uncertainty, some of it is probably real. For example around 1800 UTC day 43, the wind speed continues to fall longer than does u^* and it is reasonable to suspect that a nonequilibrium wave field is giving rise to the large $C10_N$ values after 1900 UTC. The very large scatter in Fig. 7 does not arise from short-term variability, but rather from persistent periods of lower than average $C10_N$ (e.g., day 44 0600–0900 UTC and 1300–2000 UTC) and from times of persistent large $C10_N$, such as day 43, 0000–2000 UTC.

TABLE 3. Comparison of the drag coefficient results from the DISSTRESS system during FASINEX to those from some previous studies.

Study	Wind range ($m\ s^{-1}$)	Hours of data	$10^3\ C10_N$ Mean	σ	Min	Max
Smith (1980)	6–10	~20	1.09	0.28	0.69	1.95
Large and Pond (1981)	4–10	618	1.14	0.20	0.60	1.95
Large and Pond (1982)	3–10	950	1.12	0.20	0.60	1.88
FASINEX DISSTRESS	3–10	162	1.12	0.21	0.62	1.88

The 5 h following 2000 UTC day 46 is a good example with an average $C10_N = 0.00162$, or 30% higher than expected for the average $U10 = 12\ m\ s^{-1}$ over this time. Because of these periods of systematic variation, it can take a few days or more for the average drag coefficient to converge to its long-term mean.

6. Discussion

Over the ocean, the inertial dissipation technique is well understood and well established as a viable method of measuring the scalar wind stress magnitude. This understanding enables automated systems to be built for remote applications, such as ships and buoys. The output could be a continuous time series of the neutral friction velocity, computed every 20 min. Corrections for stability could later be made from mean or bulk measurements of wind speed and sea–air temperature difference, although climatological values would suffice in some cases. A sea–air temperature difference measurement could also be incorporated into the system, allowing the stability corrections to be made internally

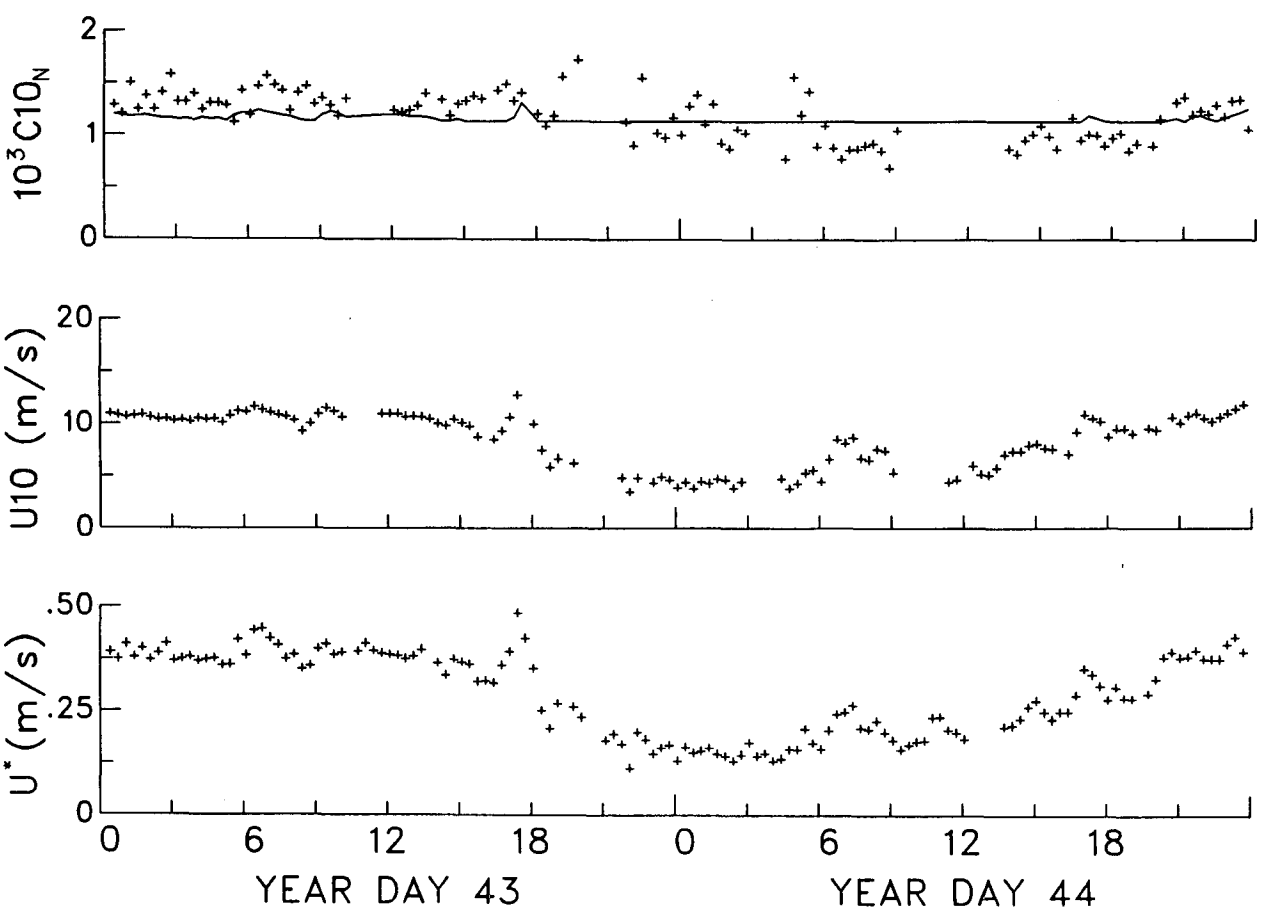

FIG. 8. Time series of friction velocity, wind speed, and drag coefficient at R/V *Endeavor* for two days during FASINEX. The solid line is $C10_N$ from the Large and Pond (1981) formulation.

in real time. However, from a ship, its velocity would need to be removed from the anemometer signal to give U_t for the stability parameter calculation.

The principal advantages of automated systems are the elimination of supervisory personnel, the much reduced post observation processing time and cost, and a greatly reduced data volume. Over 20 min the DISSTRESS system produces only five data words from its 10 Hz sampling, a 2400:1 data reduction. An optimal system could be made to produce only 1 word, a 12 000:1 reduction. The small output data rate facilitates solid state data storage and real time data telemetry. As demonstrated here, even the limited data bit rate of Service ARGOS is sufficient.

Inertial dissipation method wind stresses can differ substantially from those derived from bulk formulae (1). The difference may not be too large over periods of a few days or more, but it could be systematic. Over an hour or so it could be as much as a factor of 2. The systematic error in dissipation u^* estimates is about 3% (Large and Pond, 1981), while in bulk aerodynamic computations it could be 10% or more, depending on the wind speed measurement. The FASINEX experience showed that in many ways it was easier to measure u^* than $U10$ from a moving ship, because of problems in removing the ship's velocity from the measurement. These problems are compounded when $U10$ is squared in (1) to give the stress. Therefore, in applications where the wind stress over the ocean is needed either on short time scales, or as accurately as possible, or with a minimum systematic error, or all of the above, then a direct measurement is required. The DISSTRESS system successfully employs one technique by which such data can be obtained relatively simply.

In the system, filtering in natural frequency space enables very efficient use of computational power. It also means that to first order, the u^* corrections for sensor response (12) are independent of wind speed. Filtering in n-space also allows for other possible corrections to be made easily after the data have been taken. For example, suppose that a calibration $\hat{C}$ for a particular propeller was used to fill the wind processor look-up table, but a different propeller with calibration C was actually used, and that the anemometer was placed at height h, different from the internally stored height $\hat{h}$. The corrections to measured wind speeds, $\hat{U}$, and to $\hat{h}$ are $K_u = U/\hat{U} = \hat{C}/C$ and $K_h = h/\hat{h}$, respectively. Therefore instead of filtering between $\hat{n}_1$ and $\hat{n}_2$, the integration limits become $n_1 = K_n\hat{n}_1$ and $n_2 = K_n\hat{n}_2$, where $K_n = K_h/K_u$. The correction to u^* is $K^* = K_u K_G^{1/2}$, where K_G is the correction to the integral (9):

$$K_G = (\hat{n}_1^{-2/3} - \hat{n}_2^{-2/3})(n_1^{-2/3} - n_2^{-2/3})^{-1} = K_n^{2/3},$$

which is easily applied even after the data have been collected.

The choice between bandpass filtering and using an FFT technique is not straightforward, and in practice either could be employed. Bandpass filtering does require less processor memory, and with an optimal choice of filter orders and with $N_F = 1$, when the anemometer response is well known, it may only require about one-half as many multiplications. The FFT's advantages are that algorithms are readily available and the entire spectrum is produced. However, in order to be optimal the number of samples must be a power of 2. Now available are 16-bit, rather than the DISSTRESS 8-bit, microprocessors. Their use would greatly speed up the bandpass filtering and could allow software FFTs to be performed. Dedicated low power integrated FFT circuits may soon become available. Such technological developments make some hardware components of the DISSTRESS system obsolete and upgrades should be made before more are produced. They also make the FFT option more attractive.

Acknowledgments. We gratefully acknowledge the organizational efforts of R. A. Weller in planning and executing FASINEX. Our thanks to Ken Davidson and his group at the Naval Postgraduate School for providing their meteorological data from R/V *Endeavor.* The system was constructed by M. Neumann, with support from D. Albo and M. Carpenter of NCAR.

This work was supported primarily by the National Aeronautics and Space Administration (Grant NASA-W-15, 969), and also by the U.S. Office of Naval Research (Contract N0014-85-F-031), and by the National Science Foundation through its sponsorship of the National Center for Atmospheric Research.

REFERENCES

Busch, N. E.. 1977: Fluxes in the surface boundary layer over the sea. *Modeling and Prediction of the Upper Layers of the Oceans.* E. B. Kraus, Ed., Pergamon Press, 72–91.

Byrne, H. M., 1982: The variation of the drag coefficient in the marine surface layer due to temporal and spatial variations of the surface wind and sea state. Ph.D dissertation, University of Washington, 119 pp.

D'Asaro, E. A., 1985: The energy flux from the wind to near-inertial motions in the surface mixed layer. *J. Phys. Oceanogr.*, **15**, 1043–1057.

Dunkel, M., L. Hasse, L. Krügermeyer, D. Schriever and J. Wucknitz, 1974: Turbulent fluxes of momentum, heat and water vapor in the atmospheric surface layer at sea during ATEX. *Bound.-Layer Meteor.*, **6**, 81–106.

Evans, D. L., D. R. Watts, D. Halpern and S. Bourassa, 1984: Oceanic winds measured from the sea floor. *J. Geophys. Res.*, **89**, 3457–3461.

Fairall, C. W., and S. E. Larsen, 1986: Inertial-dissipation methods and turbulent fluxes at the air–sea ocean interface. *Bound.-Layer Meteor.*, **34**, 287–301.

Hamming, R. W., 1983: *Digital Filters.* 2nd ed., Prentic-Hall signal processing series, 257 pp.

Hasse, L., M. Gruenewald and D. Hasselmann, 1977: Field observations of air flow above the waves. *Turbulent Fluxes through the Sea Surface, Wave Dynamics and Prediction.* A. Favre and K. Hasselmann, Eds., Plenum Press.

Hellerman, S., and M. Rosenstein, 1983: Normal monthly wind stress

over the world ocean with error estimates. *J. Phys. Oceanogr.*, **13,** 1093–1104.

Khalsa, S. J S., 1980: The limitations on stress parameterization imposed by intermittency in turbulent flow. *Bound.-Layer Meteor.*, **19,** 3–17.

Large, W. G., 1979: The turbulent fluxes of momentum and sensible heat over the open sea during moderate to strong winds. Ph.D. thesis, Inst. Oceanogr. and Dept. Physics, University of British Columbia, 180 pp.

——, and S. Pond, 1981: Open ocean momentum flux measurements in moderate to strong winds. *J. Phys. Oceanogr.*, **11,** 324–336.

——, and ——, 1982: Sensible and latent heat flux measurements over the ocean. *J. Phys. Oceanogr.*, **12,** 464–482.

Lumley, J. L., and H. A. Panofsky, 1964: The structure of atmospheric turbulence. *Wiley Interscience.*

Panofsky, H. A., and J. A. Dutton, 1984: *Atmospheric Turbulence.* Wiley and Sons, Inc., 397 pp.

Pond, S., W. G. Large, M. Miyake and R. W. Burling, 1979: A gill twin propeller-vane anemometer for flux measurements during moderate and strong winds. *Bound.-Layer Meteor.*, **16,** 351–363.

Schroeder, L. C., D. H. Boggs, G. J. Dome, I. M. Halberstam, W. L. Jones, W. J. Pierson and F. J. Wentz, 1982: The relationship between wind vector and normalized radar cross section used to derive Seasat-A satellite scatterometer winds. *J. Geophys. Res.*, **87,** 3318–3336.

Smith, S. D., 1980: Wind stress and heat flux over the ocean in gale force winds. *J. Phys. Oceanogr.*, **10,** 709–726.

Wyngaard, J. C., 1981: The effects of probe-induced flow distortion on atmospheric turbulence measurements. *J. Appl. Meteor.*, **20,** 784–894.

Yaglom, A. M., 1977: Comments on wind and temperature flux–profile relationships. *Bound.-Layer Meteor.*, **11,** 89–102.